Real-Time In Vivo Imaging of Retinal Cell Apoptosis after Laser Exposure

Steffen Schmitz-Valckenberg,[1] *Li Guo,*[1] *Annelie Maass,*[1] *William Cheung,*[1] *Anthony Vugler,*[1] *Stephen E. Moss,*[1] *Peter M. G. Munro,*[1] *Frederick W. Fitzke,*[1] *and M. Francesca Cordeiro*[1,2]

Purpose. To investigate whether the detection of apoptosing retinal cells (DARC) could detect cells undergoing apoptosis in a laser model of retinal damage.

Methods. Laser lesions were placed, with the use of a frequency-doubled Nd:YAG laser, on the retina in 34 eyes of anesthetized Dark Agouti rats. Lesion size and laser-induced retinal elevation were analyzed using in vivo reflectance imaging. Development of retinal cell apoptosis was assessed using intravitreal fluorescence-labeled annexin 5 in vivo with DARC technology from baseline until 90 minutes after laser application. Histologic analysis of retinal flat mounts and cross-sections was performed.

Results. The lateral and anteroposterior depth extension of the zone of laser damage was significantly larger for higher exposure settings. A strong diffuse signal, concentrated at the outer retina, was seen with DARC for low exposures ($<$300 ms and $<$300 mW). In comparison, higher exposures ($>$300 ms and $>$300 mW) resulted in detectable hyperfluorescent spots, mainly at the level of the inner retinal layers. Dose-dependent effects on spot density and positive correlation of spot density between lesion size ($P < 0.0001$) and retinal elevation ($P < 0.0001$) were demonstrated. Histology confirmed the presence of apoptosing retinal cells in the inner nuclear and the ganglion cell layers.

Conclusions. This is the first time that DARC has been used to determine apoptotic effects in the inner nuclear layer. The ability to monitor changes spatially and temporally in vivo promises to be a major advance in the real-time assessment of retinal diseases and treatment effects. (*Invest Ophthalmol Vis Sci.* 2008;49:2773–2780) DOI:10.1167/iovs.07-1335

With the development of the confocal scanning laser ophthalmoscope (cSLO), it has become possible to image large retinal areas with increasing sensitivity, high image contrast, and superior level of resolution in the living human and the living animal eye.[1] This method has also provided a method for detecting fundus autofluorescence.[2] More recently, the authors have used the cSLO to identify single apoptosing retinal cells in vivo.[3] Until now, this technology, which we have named detection of apoptosing retinal cells (DARC), has been used to visualize retinal ganglion cell (RGC) apoptosis, with particular reference to glaucoma and its management.[3–5]

The process of apoptosis is implicated in disorders throughout the retina.[6] Apoptosis occurs in pathologic photoreceptor cell death in several mouse models of retinal degeneration, including light-induced injury and in the presence of mutations in the retinal degeneration (*rd*), retinal degeneration slow/peripherin (*rds*), and rhodopsin genes.[7–12] Apoptosis has also been shown in human blinding retinal diseases such as retinitis pigmentosa, age-related macular degeneration, pathologic myopia, diabetic retinopathy, and retinal detachment.[13–17] In these diseases, apoptotic cells may occur in multiple retinal layers, including the RGC, inner nuclear, photoreceptor, and retinal pigment epithelium cell layers and the inner choroid.[18–20]

One of the most accessible models of retinal damage is that generated by acute exposure of laser irradiation. Its application also represents one of the most important and widely used methods for the treatment of blinding eye diseases. Laser-induced retinal damage can be caused by ionization or plasma formation, thermoacoustic or mechanical transients, heat, photochemical processes, and photoablation (for a review, see Marshall[21]). These effects depend on several factors, including wavelength, pulse duration, exposure time, and laser power. Because these parameters can be standardized and easily adjusted in the experimental setting, in vivo laser radiation represents a simple and titratable model in which to study the deleterious effects of acute damage on the retina.

Characteristics of laser-induced retinal damage have been extensively studied histologically.[22–29] Laser exposure has been reported to produce apoptosis in kangaroo kidney epithelium and retinal pigment epithelium cell cultures.[30,31] The development of retinal apoptosis by exposure to high light levels in the animal model has been well established in vitro.[32] In these models, it appears that photoreceptor apoptosis is mediated by rhodopsin and is wavelength dependent.[11,33] More recently, Matsubara et al.[34] have shown histologic apoptotic changes in choroidal neovascularization induced by photodynamic therapy. Methods relying on postmortem analysis do not enable effects to be monitored in real time, and it is still unknown how much alteration of intrinsic activity occurs as a result of tissue fixation and processing. Visualization of real-time in vivo apoptosis in the living eye or detailed analysis of apoptotic processes in vivo has not previously been possible.

A widely used apoptosis marker is the protein annexin 5.[35] In the presence of Ca^{2+}, this molecule has a high affinity for phosphatidylserine, an anionic phospholipoid that is enriched in the inner leaflet of plasma membranes. In the early development stages of apoptosis, annexin 5 is externalized from the inner to the outer cell membrane, before DNA fragmentation and nuclear condensation occur. Using radiologic and fluorescent techniques, annexin 5 has been shown to be effective in the identification of apoptosis in vivo and in vitro.[3,35–40]

From the [1]Institute of Ophthalmology, University College London, London, United Kingdom; and [2]Western Eye Hospital, London, United Kingdom.

Supported by Sharp-Eye Research Fellowship; European Commission FP5, HPRN-CT-2002-00301; Foundation Fighting Blindness; and Wellcome Trust.

Submitted for publication October 17, 2007; revised January 15, 2008; accepted April 11, 2008.

Disclosure: **S. Schmitz-Valckenberg**, None; **L. Guo**, None; **A. Maass**, None; **W. Cheung**, None; **A. Vugler**, None; **S.E. Moss**, None; **P.M.G. Munro**, None; **F.W. Fitzke**, None; **M.F. Cordeiro**, None

Presented in part at the annual meeting of the Association for Research in Vision and Ophthalmology, Fort Lauderdale, Florida, May 2007.

The publication costs of this article were defrayed in part by page charge payment. This article must therefore be marked "*advertisement*" in accordance with 18 U.S.C. §1734 solely to indicate this fact.

Corresponding author: M. Francesca Cordeiro, UCL Institute of Ophthalmology, 11-43 Bath Street, London, EC1V 9EL, United Kingdom; m.cordeiro@ucl.ac.uk.

In this study, we investigated real-time in vivo retinal apoptosis after laser radiation using the DARC technique with fluorescence-labeled annexin 5.

Materials and Methods

Animals

All procedures were approved by the United Kingdom Home Office and complied with the ARVO Statement for the Use of Animals in Ophthalmic and Vision Research. Thirty-four adult male Dark Agouti rats, each weighing 200 to 250 g, were anesthetized by intraperitoneal injections of ketamine (37.5%)/medetomidine hydrochloride (25%; Domitor; Pfizer Animal Health, Exton, PA) solution (0.75 mL ketamine, 0.5 mL medetomidine hydrochloride, and 0.75 mL sterile water) at 0.2 mL/100 g. Pupils were dilated with 2.5% phenylephrine hydrochloride and 1.0% tropicamide (Chauvin Pharmaceuticals Ltd., Surrey, UK). For this study, human recombinant annexin 5 was labeled with infrared imaging reagent (IRDye; LI-COR Biosciences, Lincoln, NE; 800CW; absolute maximum, 774; emission maximum, 789) according to manufacturer's instructions and delivered by way of the intravitreal route, as described previously.[3–5,41]

Laser Exposure

One hour after injection of annexin 5, laser lesions were focused on the retina with a green, frequency-doubled, solid-state Nd:YAG laser at $\lambda = 532$ nm (IRIS Medical OcuLight GL, Carlton Ltd., Buckinghamshire, UK). An indirect ophthalmoscope and a 20-diopter (D) lens were applied to visualize the aiming beam. The spot size, which encompassed roughly 1 to 2 disc areas (DAs), was not changed during the study. Visible lesions were observed with all laser settings used. Care was taken to ensure laser lesions were clearly separated so that borders did not overlap or coalesce. Exposure time and laser power were varied from 100 ms and 100 mW to 500 ms and 500 mW, respectively. Animals were imaged at baseline and immediately after laser application.

In Vivo Imaging

All in vivo imaging was carried out using our recently described DARC technique with a modified cSLO (Heidelberg Retina Angiograph 2, Heidelberg Engineering, Dossenheim, Germany). The standard lens (15° × 15°–30° × 30°) and the wide-field lens (55°; all degree values calibrated for the human eye) were used.[3,4,41] Reflectance and corresponding fluorescence images with different focus settings were taken of the rat retina. Because of the confocal optics, this approach allows the acquisition of sectional scans through the rat retina for investigation of the depth location of the detected fluorescence signal.[42,43] Although the depth resolution is limited, the nerve fiber layer is distinguishable from the inner and outer retinal layers. To improve the signal-to-noise ratio and to enhance image contrast, the mean image out of a series of single images (up to 100) was calculated after correction of eye movements.

Image Analysis

With image analysis software, the individual pixel distribution of each image was optimized by changing image contrast and brightness (Adobe Photoshop 7.0; Adobe Systems Inc., Mountain View, CA). The area of laser burns was measured by manually outlining the borders of each lesion at the outer retina with the mouse-driven arrow on the reflectance images. In addition, the optic disc for each eye was outlined, and lesion areas were subsequently calculated in disc area. In the rat eye, 1 DA roughly corresponds to 0.041 mm^2, assuming a lateral pixel resolution of 1.15 μm/pixel.[41] Each focal plane of the cSLO is defined by the diopter units of the focus settings. To investigate retinal elevation after treatment, the relative anteroposterior depth extension of damage was quantified by the differences of diopter units between the scans at the level of the nerve fiber layer and the outer retina (retinal pigment epithelium/photoreceptor complex) at the center of the laser burn. According to Hughes, the axial length in Dark Agouti rats is 6.3 mm compared with approximately 24 mm in a human eye.[44] An estimation of 1 D in a rat eye would be roughly 20 μm. This approximation would be consistent with the comparison of retinal thickness between cSLO in vivo imaging and confocal microscopy on postmortem cross-sections (taking 10% shrinkage into account) over nonexposed retinal areas in this study. The number of apoptotic cells labeled by annexin 5 was counted on the fluorescence scans. The amount of apoptosis was analyzed by spot density per DA (number per lesion size area).

Histologic Analysis

After laser exposure and subsequent cSLO imaging for up to 90 minutes, animals were killed and eyes were immediately enucleated. Eyes were fixed in 4% paraformaldehyde overnight and processed for either retinal flat mounts or cryostat cross-section analysis. For the latter, eyes were cryoprotected with 30% sucrose solution (in 0.1 M PBS), embedded in OCT compound (Tissue-Tek; Sakura Finetek, Tokyo, Japan), and frozen in acetone solution. The frozen blocks were then cut into sections 20 μm thick and were stained with 4,6-diamidino-2-phenylindole (DAPI, 1:2500; Sigma-Aldrich, St. Louis, MO) for assessment of nuclei and identification of retinal layers. For flat mounts, eyes were dissected at the equator, and the lens and vitreous were removed. Flat retinas were obtained and mounted in glycerol/PBS solution. Cross-sections and flat mounts were assessed by using a confocal laser scanning microscope (LSM 510 UV; Zeiss, Thornwood, NY) with LSM software.

Furthermore, two eyes were fixed with 3% glutaraldehyde and 1% paraformaldehyde in 0.08 M sodium cacodylate-HCl buffer (pH 7.4), rinsed three times in PBS, and immersed in 1% aqueous osmium tetroxide solution for 2 hours at room temperature. Tissue was then rinsed in distilled water (three times), dehydrated by 15-minute incubations in 50%, 70%, and 90% 3 × 100% ethanol, 2 × 20-minute changes of propylene oxide, and left overnight in a 1:1 mixture of propylene oxide/araldite to infiltrate. This was changed for full resin and left on a rotator for 6 hours before embedding and overnight polymerization at 60°C. Semithin sections for examination by light microscopy were cut using a Leica (Wetzlar, Germany) ultracut S microtome and diamond knife, stained with a mixture of 1% borax and 1% toluidine blue in 50% ethanol at 60°C, dried, and mounted in xylene. Ultrathin sections were cut at 70 nm thickness, stained with lead citrate, and viewed under a transmission electron microscope (JEOL 1010; JEOL, Tokyo, Japan) operating at 80 kV. Images were recorded onto film (4489 EM; Eastman Kodak, Rochester, NY) and later digitized with a flat bed scanner (DuoScan T2500; Agfa, Brentford, Middlesex, UK). All stains and resins were supplied by Agar Scientific Ltd. (Stansted Essex, UK).

Statistical Analysis

Statistical analyses included frequency and descriptive statistics. Three energy settings were used for comparison of laser exposure effects: 100 ms and 100 mW, 300 ms and 300 mW, 500 ms and 500 mW. The Kruskal-Wallis test was used for statistical analysis between treatments (SPSS 11.0; SPSS, Chicago, IL). Mean results and 95% confidence intervals were displayed graphically. The relation between the spot density and the lateral and anteroposterior extensions of damage was investigated using the Spearman rank correlation coefficient (ρ). $P < 0.05$ was considered statistically significant.

Results

Placement of Laser Lesions

Five to six laser lesions were placed around the disc (Fig. 1). For all exposure settings, in vivo reflectance imaging showed sharply demarcated, circular lesions with rapid enlargement

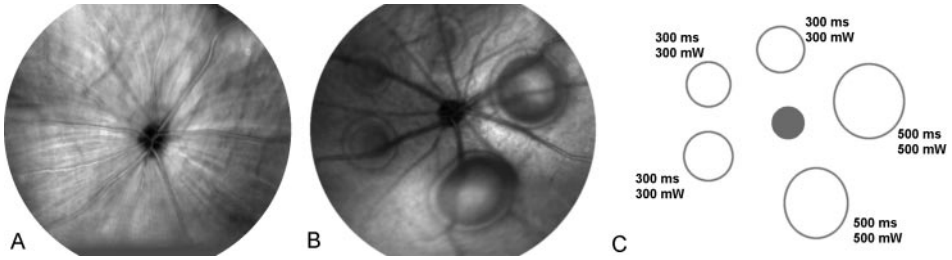

FIGURE 1. Placement of laser lesions in rat eye. (**A**) Baseline reflectance image before laser exposure is focused at the level of the nerve fiber layer. Normal central retina is visualized. (**B**) Five to six laser lesions were placed around the disc. Reflectance imaging immediately after laser exposure shows five laser burns. (**C**) Schematic drawing illustrates the different exposure settings. Note the larger lesion size and the marked development of a blister for the burns with higher exposures (**B**, **C**).

and swelling at the borders. Depending on the intensity settings, different retinal damage characteristics were observed at the site of the laser burn immediately after treatment. Characteristically, at low settings (100 ms and 100 mW), mild whitening and discoloration were observed, and at higher settings lesions appeared more creamy and chalky white. At the highest settings (500 ms and 500 mW), the rapid development of a blister in the center of the laser burn was usually observed at the end of the application. However, no subretinal hemorrhages were observed in any type of laser burn.

In Vivo Imaging and Spatial Assessment of Retinal Damage on the Effects of Different Levels of Laser Exposure

For all levels of laser exposure, the area of the laser burns was greatest and most pronounced in the outer retina in the reflectance images (Fig. 2). Overall, the median lesion size at the outer retina was 4.0 DA (interquartile range [IQR], 2.9–7.2). The median anteroposterior extension of damage was 18.0 D (IQR, 14.3–24.0) compared with a median retinal thickness of 13.2 D (IQR, 11.2–15.0) before laser application. A dose-dependent correlation of the spatial extension of the zone of damage was observed (Fig. 3). The lesion size area for the group with low energy settings (100 ms and 100 mW) was always less than 1 DA, and no retinal elevation compared with baseline was detectable ($P = 0.52$). Laser lesions produced with higher settings (300 ms and 300 mW) were significantly larger ($P = 0.004$) and showed increased retinal thickness ($P = 0.006$). Blister formation with even more lateral ($P = 0.008$) and anteroposterior ($P = 0.014$) extension of damage was seen for the highest settings (500 ms and 500 mW).

In Vivo Imaging and Assessment of Cell Apoptosis for Different Laser Exposures

Fluorescence scans revealed dose-dependent effects on the spatial distribution and uptake of fluorescence-labeled annexin 5 (Fig. 2). Low settings ($\leq$ 200 ms and $\leq$ 200 mW) produced diffuse hyperfluorescence at the site of the laser lesion. This strong signal of the label was concentrated at the outer retina. However, no distinct apoptosing spots were observed. Energy settings of 300 ms and 300 mW produced diffuse hyperfluorescence at the edges of the lesion, at the level of the outer

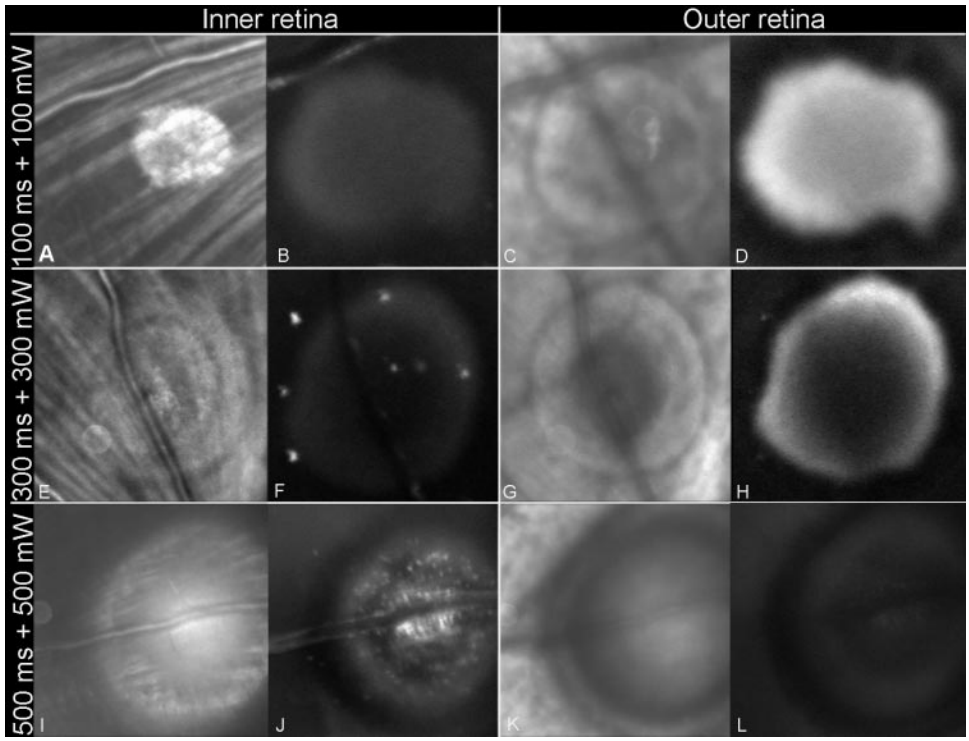

FIGURE 2. In vivo imaging on the effects of different levels of laser exposure. Reflectance imaging (confocal plane: **A**, **E**, **I**, inner retina; **C**, **G**, **K**, outer retina) shows that the size of the laser lesions is dose dependent and that the lateral extension of damage is larger at the outer retina. Fluorescence imaging (corresponding focal planes to the reflectance images: **B**, **F**, **J**, inner retina; **D**, **H**, **L**, outer retina) visualizes distribution and uptake of fluorescence-labeled annexin 5. Within the burn produced with the lowest settings (100 ms and 100 mW; **A–D**, *top row*), an intense diffuse hyperfluorescence is detected. Confocal imaging suggests that this signal is mainly derived from the outer retina (**D**). Laser intensities at 300 ms and 300 mW (**E–H**) produce diffuse hyperfluorescence at the edges of the lesion at the level of the outer retina (**H**) and a few spots inside and near the lesion at the level of in the inner retina (**F**). Increasing the power and exposure time (500 ms and 500 mW, **I–L**) reveals many hyperfluorescent spots, concentrated in the middle of the lesion, that are visualized in the presence of blister formation at the level of the inner retina (**J**).

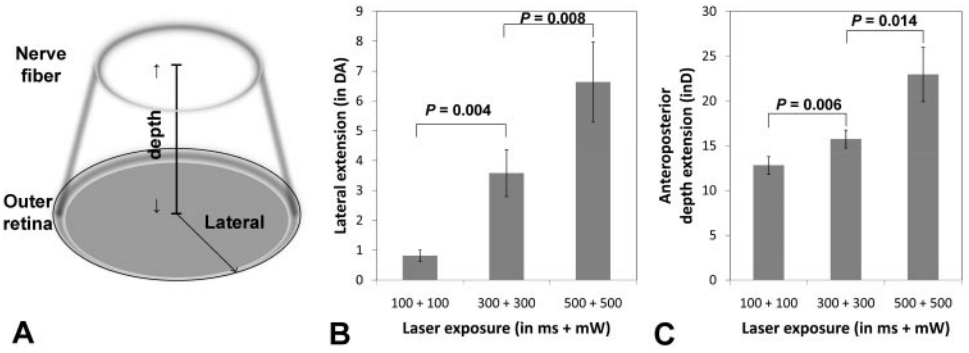

FIGURE 3. Spatial assessment of retinal damage and the effects of different levels of laser exposure. (**A**) The extent of laser damage was defined by two parameters. The lateral extension was assessed at the level of the outer retina, where it was measured in DA. The relative anteroposterior depth extension was quantified by the differences in diopter units between scans of the inner retina and outer retina. (**B**, **C**) A dose-dependent correlation of the spatial extension of the zone of damage was observed. The lesion size area for the group with low-energy settings (100 ms and 100 mW) was always less than 1 DA, and no significant retinal elevation compared with baseline was detectable ($P = 0.52$). Laser lesions produced with higher settings (300 ms and 300 mW) were significantly larger ($P = 0.004$) and showed increased retinal thickness ($P = 0.006$). Blister formation with even more lateral ($P = 0.008$) and anteroposterior depth ($P = 0.014$) extension of damage was seen for the highest settings (500 ms and 500 mW).

retina. Few spots inside and near the lesion at the level of the inner retina were observed within 20 minutes after laser application. The highest exposure levels (500 ms and 500 mW) showed many hyperfluorescent spots. Their density was typically found to be highest at the center of the lesion and at the level of the inner retina. Some spots were also seen at the edges or in the direct vicinity of the lesions.

Approximately 1 hour after laser exposure, spot density at the inner retina was significantly higher for the 500-ms and 500-mW group (median, 12.1 per DA) compared with the 300-ms and 300-mW group (1.66 per DA; $P = 0.007$; Fig. 4). When lateral and anteroposterior depth assessments of damage were plotted against the spot density, a positive correlation for higher spot density in lesions with larger lesion areas ($P < 0.0001$; $\rho = 0.75$) and with more pronounced retinal elevation ($P < 0.0001$; $\rho = 0.77$) was observed.

In Vivo Analysis of Blister Lesion

Confocal live scanning through lesions with blister formation at 500 ms and 500 mW allowed more detailed assessment of spot location (Fig. 5). At the most anterior parts of these lesions, where the RGC layer is located, only a few hyperfluorescent spots were detected. In fact, most discrete spots were located slightly more deeply; maximum apoptotic cell number was seen at the level at which the inner nuclear retina would be assumed. Subsequent scans of more posterior planes at the outer retina showed a fading fluorescence signal with no discrete spots visible.

Histologic Assessment of Retinal Damage and Apoptosis

Confocal Histologic Analysis of Whole Retina. Through an approach similar to in vivo confocal analysis, retinal flat mounts were assessed with the use of confocal scanning laser fluorescence microscopy (Fig. 6). Imaging of all laser burns revealed sharply demarcated circular zones of damage. At the outer retinal layers, massive tissue destruction and diffuse signals with no visible anatomic details, including hyperfluorescent spots, were detected inside the burns. However, lesions with high exposure settings showed hyperfluorescent spots at the level of the inner retina of the specimen. Spots were most numerous at the center, and spot density appeared to be highest at the level of the inner nuclear layer. Markedly fewer spots were seen at the RGC layer. These results were consistent with those of the in vivo study.

Morphologic Cross-Sectional Analysis with Light and Electron Microscopy. Cross-sectional analysis with the use of light and transmission electron microscopy showed characteristic structural changes at the site of the laser lesions (Fig. 7). For low settings, damage was confined to the outer retina, with photoreceptor displacement, disruption of outer segments, and necrotic and vacuolar debris inside the retinal pigment epithelial cells. Bruch membrane appeared to be intact. For high-energy burns, zones of damage were larger, and damage extended to both the choriocapillaris and the more inner retinal layers. Extensive disruption and vacuolization of the retinal pigment epithelium and choriocapillaris were present. In the middle of lesions with maximum exposure parameters, distortion of photoreceptor outer segments with elevation toward the vitreous, disruption of the inner nuclear layer with pyknotic nuclei, abnormal distribution of heterochromatin, local swelling of the cytoplasm, and organelle loss were seen. The edges showed folding of photoreceptor and inner nuclear layers. These structural changes were consistent with the formation of a blister after laser radiation.[28,29]

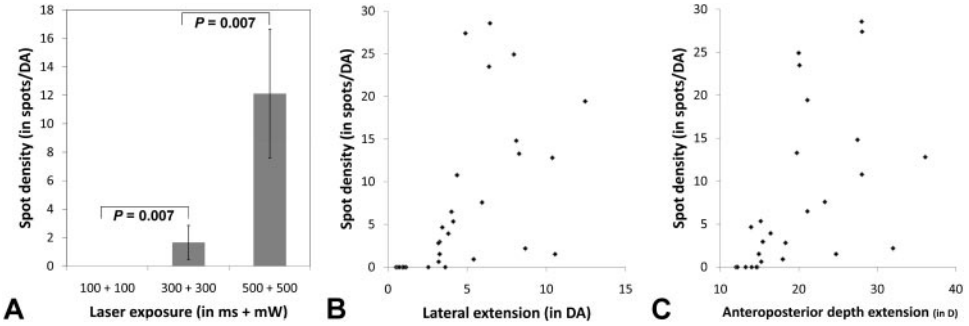

FIGURE 4. Assessment of retinal cell apoptosis for different laser exposures in vivo. (**A**) No retinal cell apoptosis inside the laser burn was observed for 100 mW and 100 ms. For the other two energy groups, the density of spots per DA (number of spots per disc area) was significantly higher in the 500 ms and 500 mW group than in the 300 ms and 300 mW group (see also Fig. 2). (**B**, **C**) For each lesion, both the lateral and the anteroposterior extension of damage were plotted against the spot density. The two graphs show a positive correlation for higher spot density in lesions with larger lesion size and with more pronounced retinal elevation. These findings were statistically significant (Spearman rank coefficient; each $P < 0.0001$).

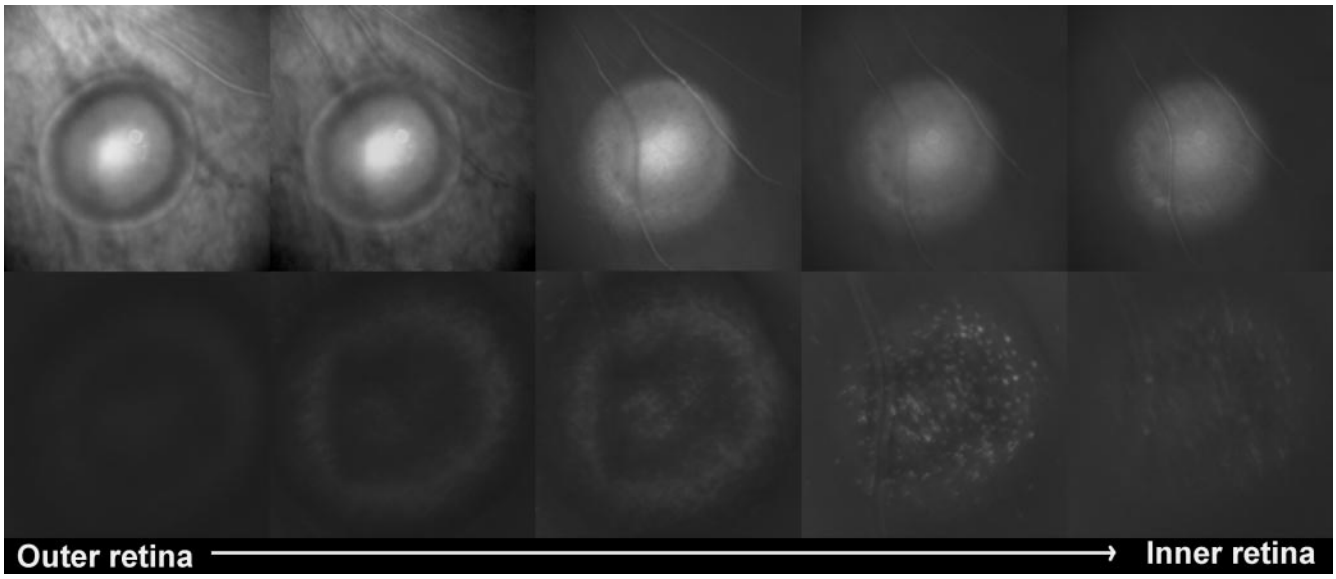

FIGURE 5. In vivo analysis of blister lesion. This sequence of five reflectance images (*upper line*) with corresponding fluorescence (*lower line*) images illustrates sectional scans through a laser blister (500 ms and 500 mW). Scanning from the outer retina (*far left*) toward the vitreous to the anterior part of the lesion (*far right*), the reflectance mode reveals a circular, well-demarcated zone of damage with surrounding edema. The fluorescence mode shows mild intensity at the outer retina, whereas hyperfluorescent spots are imaged at the more inner retinal layers. The density of these spots appears to be highest at the inner retina, at the level below the ganglion cell layers and most probably at the inner nuclear layer.

Cross-Section Analysis of Retinal Apoptosis. Cross-section histologic analysis using the cryostat technique allowed for better depth resolution of retinal cell apoptosis within the laser lesions (Fig. 8). Few marked hyperfluorescent spots were observed at the superficial retina corresponding to RGCs, and most spots were seen at the level of the inner nuclear layer showing nuclei colocalization. The photoreceptor nuclei layer did not show any annexin 5-positive staining.

DISCUSSION

This is the first time, to our knowledge, that laser-induced retinal cell apoptosis in the inner nuclear layer has been demonstrated in vivo. Until now, the DARC technique has been only used to investigate RGC apoptosis. In addition, our study clearly showed that it is possible to quantify dose-dependent effects on both the development of apoptosing cells in vivo and the spatial extent of retinal damage.

Our demonstration of apoptosis within 20 minutes of laser application supports the view that annexin 5 is a marker of early apoptosis, detecting cell death significantly earlier than other methods.[35,45] Our observations are also in accordance with a recent report by Matsubara et al.,[3] who demonstrated the presence of apoptotic cells after the first hour of photodynamic therapy in a laser-induced CNV rat model. Apoptosis in their study was identified immunohistochemically with the use of TUNEL assay and caspase activation markers. Previous studies using the DARC technique have confirmed histologically that annexin 5-positive cells show double-labeling with anti-caspase-3.[22–29] In this study, in vivo apoptosis imaging was limited to 90 minutes after laser application. We observed a slight increase in hyperfluorescent spots over time in a few laser burns. However, because of time-consuming imaging of several laser burns and imaging of different layers, no systematic analysis or quantification of changes in spot numbers within the observation period was possible and would have extended beyond the scope of the study. In comparison with histologic analysis, the DARC technique offers the possibility of investigating cellular changes as they occur, in real-time and in the same animal over a period of hours, days, weeks, or even longer. This has implications not only with regard to the number of animals required but also with respect to the assessment of apoptotic processes and treatment efficacy.

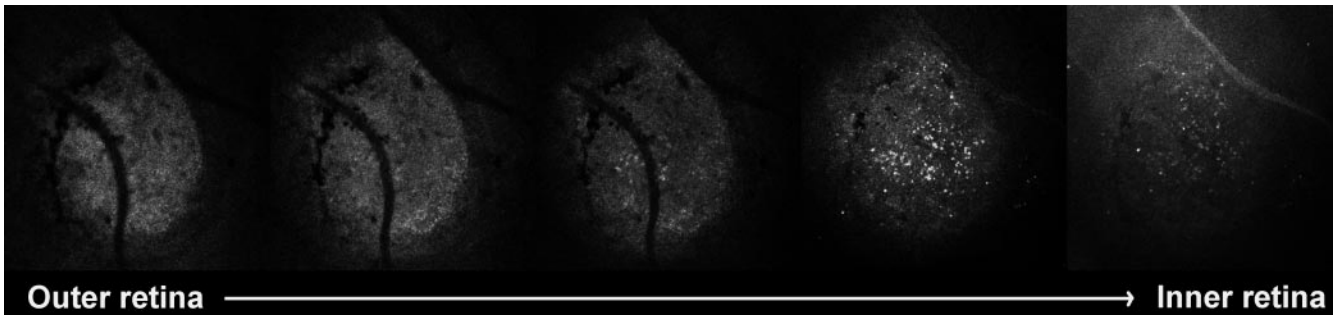

FIGURE 6. Confocal histologic analysis of whole retina. Confocal histologic analysis of whole retina of a blister lesion (exposure settings: 500 ms and 500 mW) reveals massive destruction and loss of anatomic details with mildly diffuse hyperfluorescence at the outer retina. Hyperfluorescent spots are visualized at the level of the inner retina. The number of spots is highest in the middle of the lesion and at the inner nuclear layer. Markedly fewer spots are seen at the ganglion cell layers. These results were consistent with the in vivo imaging analysis.

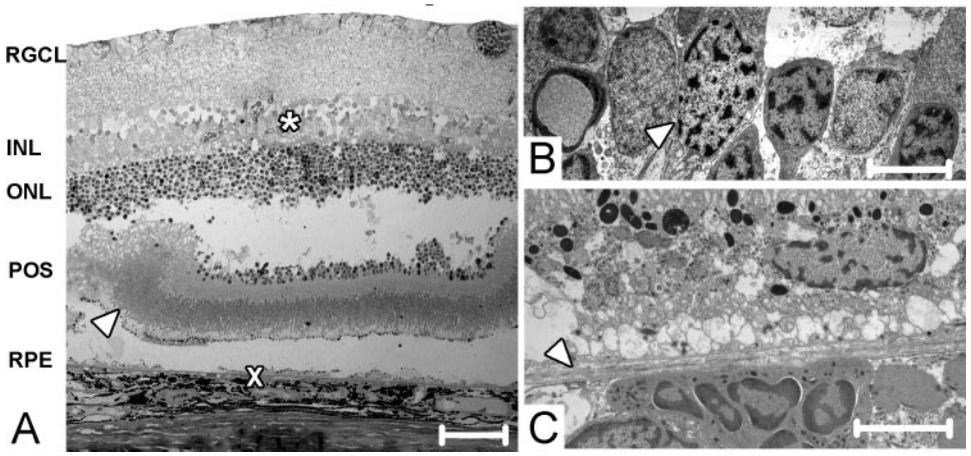

FIGURE 7. Morphologic cross-sectional analysis with light and electron microscopy. Representative cross-sections through laser lesion (500 ms and 500 mW) with light and transmission electron microscopy. (**A**) Semithin section (3 μm in thickness) through the laser burn reveals the formation of a blister. Elevation of the photoreceptor outer segments (POS), separation of the outer nuclear layer (ONL), and disruption of the inner nuclear layer (INL) are observed. No pronounced damage is visible at the level of the retinal ganglion cell (RGCL). At the edge of the burn (*far left*, *arrowhead*), folding of the photoreceptor outer segment layer is present. Scale bar, 50 μm. (**B**) Electron transmission microscopy photographs (×2500; *approximate location) show structural changes consistent with apoptosis, including pyknotic nuclei (*arrowhead*) with abnormal distribution of heterochromatin, local swelling of the cytoplasm, and organelle loss in the INL. (**C**) Electron microscopy (x) shows disruption and vacuolization at the retinal pigment epithelium and choriocapillaris level. Bruch membrane (*arrowhead*) appears to be intact.

Our funduscopic and histopathologic observations of structural changes after laser exposure are in keeping with previous reports evaluating the effects of laser irradiation, including the primary site of damage and dose-dependent involvement of different retinal layers.[46–50] We have confirmed that the application of the minimal laser energy required for producing a visible lesion correlated with histologic retinal damage limited to the outer retina and choroid with intact Bruch membrane. Higher settings were associated with retinal elevation and involvement of more inner retinal structures, extending to the RGC layer. Retinal disruption and blister formation are known to occur with high laser intensities and have been previously shown to be more common with the frequency-doubled Nd:YAG laser than with the argon laser.[49] These structural changes after laser radiation are thought to be induced by acoustic or thermo-mechanical shock waves rather than simple thermal effects.[51,52]

Different interactions between the laser light and the retina could explain the phenomena observed in this study. We believe that localized damage and no visible retinal elevation associated with low-energy settings were produced mainly by thermal melting and acute necrotic effects. Acute damage with photoreceptor disruption and exposure of cellular debris in the outer retina, including the inner lipid membranes containing phosphatidylserine, might have led to pooling of annexin 5, as identified in in vivo images by markedly diffuse fluorescence at the outer retina (Fig. 2). This could explain why, during tissue processing, this (pooled) annexin 5 would have been washed out and not detectable histologically. Washing out of material during processing is thought to be responsible for differences between in vivo and histologic observations in other retinal conditions, such as the absence of yellow vitelliform material in histologic sections through "egg yolk" lesions seen on funduscopy in patients with Best disease.[53] The elution of material in Best disease is supported by an observation made by Eckardt et al.[31] during macular translocation on a patient with adult vitelliform macula dystrophy. While surgically removing the vitelliform lesion en bloc, they noticed that the yellow vitelliform material was washed out during processing.

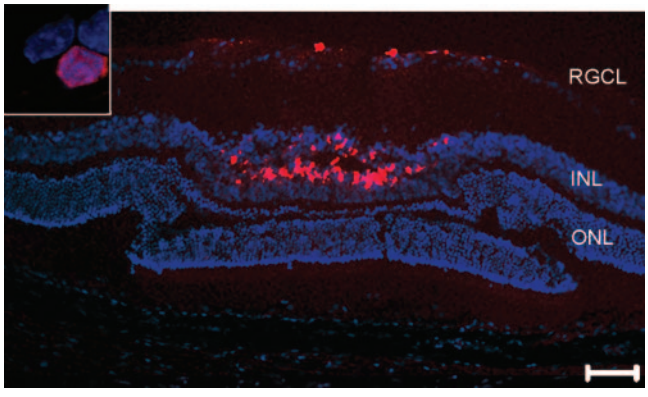

FIGURE 8. Cross-sectional analysis of retinal apoptosis. Cryostat cross-sectioning through a histologic laser lesion (energy setting: 500 ms and 500 mW) and overlay with DAPI allows for localization of annexin 5-positive spots mainly at the inner nuclear layer (INL) (*blue*, DAPI; *red*, fluorescence-labeled annexin 5). Few spots are present at the ganglion cell layer (RGCL). High magnification of the inner nuclear layers (*inset*) shows colocalization of annexin 5-positive spots (*red*) with cell nuclei (*blue*). Scale bar, 50 μm.

With increasing exposure time and laser power, acute retinal damage appeared to involve more inner retinal layers with tissue disruption and blister formation. At the outer retina, these high energies might have resulted in coagulative necrosis, thus fixing the cellular membranes of the photoreceptors in place so that they could not react with annexin 5. The reduced energy at the edge of the lesion might have resulted in less damage, similar to that at the center of burns with 100 ms and 100 mW, manifesting as a hyperfluorescent ring in vivo and no histopathologic correlate because of washout phenomena. By contrast, in the inner retina, no massive destruction was seen, but structural changes consistent with apoptotic processes were. This explains why it was possible to identify apoptosis at this level, as supported by the observation of hyperfluorescent spots at the inner retina, but suggests that a different mode of damage was responsible for the different effects. This is consistent with the assumption that the damage induced at the inner retina with higher laser settings is caused by thermoacoustic or mechanical, as opposed to thermal, transients. Additional mechanisms may also include (at least transiently) ischemia of the inner retina.

In one previous report on the effects of laser irradiation on apoptosis in retinal pigment epithelial cell cultures, Barak et al.[32] reported massive destruction at the center of the laser burn and the occurrence of apoptosis at the periphery of the lesion. These results would be in accordance with the development of massive necrosis in the middle of the laser burn at

the outer retina and the development of apoptosis further away from the primary site of damage in the present study.

We did not observe photoreceptor apoptosis in our study. Photochemical reactions are thought to be responsible for photoreceptor apoptosis in several light-induced models.[32] It can be assumed that acute, intense laser exposure resulted in the necrosis and cell death of photoreceptors before any photochemical reactions could have developed. We suggest more appropriate models with reduced light intensity and longer exposure times would be required to investigate whether DARC can visualize real-time in vivo apoptosis in photoreceptors.

The observation of cell apoptosis with high exposure settings also confirms current clinical guidelines. Regardless of the desired treatment effect, retinal elevation and blister formation are indicative of laser overexposure and are considered early markers of laser-induced subretinal hemorrhage.[49] The development of apoptosis in the inner nuclear and RGC layers would be an additional reason to decrease intensity settings before further application of laser burns. Our results also demonstrate that the extension of the visible laser lesion size may be correlated with the amount of apoptosing cells. This finding underscores the importance of carefully controlling lesion size during retinal laser application.

In summary, we could observe individual apoptosing spots after suprathreshold laser exposure in vivo using DARC and histologic examination. These observations are suggestive of ongoing retinal cell death, mainly in the inner nuclear layer. DARC has previously been used to delineate RGC changes. This is the first time this technique has been used to determine effects on other retinal cells. Our study demonstrated that DARC may be used to image real-time retinal cell apoptosis after laser damage. The ability to monitor changes as they occur and longitudinally as they progress promises to be a major advance in the real-time assessment of retinal diseases and treatment effects.

Acknowledgments

The authors thank Pete Coffey for his support in part of the postmortem analysis; Vy Luong for technical support; Carleton Limited (Buckinghamshire, UK) for providing the laser device; Olivier Clarke and Paul Browne (Carl Zeiss UK Ltd.) for technical support; and Francoise Russo-Marie for her scientific support.

References

1. Webb RH, Hughes GW, Delori FC. Confocal scanning laser ophthalmoscope. *Appl Optics*. 1987;26:1492–1499.
2. von Ruckmann A, Fitzke FW, Bird AC. Distribution of fundus autofluorescence with a scanning laser ophthalmoscope. *Br J Ophthalmol*. 1995;79:407–412.
3. Cordeiro MF, Guo L, Luong V, et al. Real-time imaging of single nerve cell apoptosis in retinal neurodegeneration. *Proc Natl Acad Sci U S A*. 2004;101:13352–13356.
4. Guo L, Salt TE, Luong V, et al. Targeting amyloid-β in glaucoma treatment. *Proc Natl Acad Sci U S A*. 2007;104:13444–13449.
5. Guo L, Salt TE, Maass A, et al. Assessment of neuroprotective effects of glutamate modulation on glaucoma-related retinal ganglion cell apoptosis in vivo. *Invest Ophthalmol Vis Sci*. 2006;47:626–633.
6. Kermer P, Bahr M. [Programmed cell death in the retina: molecular mechanisms and therapeutic strategies]. *Ophthalmologe*. 2005;102:674–678.
7. Chang GQ, Hao Y, Wong F. Apoptosis: final common pathway of photoreceptor death in rd, rds, and rhodopsin mutant mice. *Neuron*. 1993;11:595–605.
8. Harada T, Harada C, Nakayama N, et al. Modification of glial-neuronal cell interactions prevents photoreceptor apoptosis during light-induced retinal degeneration. *Neuron*. 2000;26:533–541.
9. Perche O, Doly M, Ranchon-Cole I. Caspase-dependent apoptosis in light-induced retinal degeneration. *Invest Ophthalmol Vis Sci*. 2007;48:2753–2759.
10. Portera-Cailliau C, Sung CH, Nathans J, Adler R. Apoptotic photoreceptor cell death in mouse models of retinitis pigmentosa. *Proc Natl Acad Sci U S A*. 1994;91:974–978.
11. Reme CE, Grimm C, Hafezi F, Marti A, Wenzel A. Apoptotic cell death in retinal degenerations. *Prog Retin Eye Res*. 1998;17:443–464.
12. Sanges D, Comitato A, Tammaro R, Marigo V. Apoptosis in retinal degeneration involves cross-talk between apoptosis-inducing factor (AIF) and caspase-12 and is blocked by calpain inhibitors. *Proc Natl Acad Sci U S A*. 2006;103:17366–17371.
13. Dunaief JL, Dentchev T, Ying GS, Milam AH. The role of apoptosis in age-related macular degeneration. *Arch Ophthalmol*. 2002;120:1435–1442.
14. Nakazawa T, Hisatomi T, Nakazawa C, et al. Monocyte chemoattractant protein 1 mediates retinal detachment-induced photoreceptor apoptosis. *Proc Natl Acad Sci U S A*. 2007;104:2425–2430.
15. Cook B, Lewis GP, Fisher SK, Adler R. Apoptotic photoreceptor degeneration in experimental retinal detachment. *Invest Ophthalmol Vis Sci*. 1995;36:990–996.
16. Arroyo JG, Yang L, Bula D, Chen DF. Photoreceptor apoptosis in human retinal detachment. *Am J Ophthalmol*. 2005;139:605–610.
17. Barber AJ, Lieth E, Khin SA, Antonetti DA, Buchanan AG, Gardner TW. Neural apoptosis in the retina during experimental and human diabetes: early onset and effect of insulin. *J Clin Invest*. 1998;102:783–791.
18. Ferrington DA, Tran TN, Lew KL, Van Remmen H, Gregerson DS. Different death stimuli evoke apoptosis via multiple pathways in retinal pigment epithelial cells. *Exp Eye Res*. 2006;83:638–650.
19. Sparrow JR, Nakanishi K, Parish CA. The lipofuscin fluorophore A2E mediates blue light-induced damage to retinal pigmented epithelial cells. *Invest Ophthalmol Vis Sci*. 2000;41:1981–1989.
20. Suter M, Reme C, Grimm C, et al. Age-related macular degeneration: the lipofusion component N-retinyl-N-retinylidene ethanolamine detaches proapoptotic proteins from mitochondria and induces apoptosis in mammalian retinal pigment epithelial cells. *J Biol Chem*. 2000;275:39625–39630.
21. Marshall J. Lasers in ophthalmology: the basic principles. *Eye*. 1988;2(suppl):S98–S112.
22. Bresnick GH, Frisch GD, Powell JO, Landers MB, Holst GC, Dallas AG. Ocular effects of argon laser radiation, I: retinal damage threshold studies. *Invest Ophthalmol*. 1970;9:901–910.
23. Leibu R, Davila E, Zemel E, Bitterman N, Miller B, Perlman I. Development of laser-induced retinal damage in the rabbit. *Graefes Arch Clin Exp Ophthalmol*. 1999;237:991–1000.
24. L'Esperance FA Jr, Kelly GR. The threshold of the retina to damage by argon laser radiation. *Arch Ophthalmol*. 1969;81:583–588.
25. Marshall J, Hamilton AM, Bird AC. Histopathology of ruby and argon laser lesions in monkey and human retina: a comparative study. *Br J Ophthalmol*. 1975;59:610–630.
26. Smiddy WE, Fine SL, Quigley HA, Hohman RM, Addicks EA. Comparison of krypton and argon laser photocoagulation: results of stimulated clinical treatment of primate retina. *Arch Ophthalmol*. 1984;102:1086–1092.
27. Marshall J, Mellerio HJ. Histology of retinal lesions produced with Q-switched lasers. *Exp Eye Res*. 1968;7:225–230.
28. Marshall J, Mellerio J. Pathological development of retinal laser photocoagulations. *Exp Eye Res*. 1967;6:303–308.
29. Marshall J, Mellerio J. Histology of the formation of retinal laser lesions. *Exp Eye Res*. 1967;6:4–9.
30. Tirlapur UK, Konig K, Peuckert C, Krieg R, Halbhuber KJ. Femtosecond near-infrared laser pulses elicit generation of reactive oxygen species in mammalian cells leading to apoptosis-like death. *Exp Cell Res*. 2001;263:88–97.
31. Barak A, Goldkorn T, Morse LS. Laser induces apoptosis and ceramide production in human retinal pigment epithelial cells. *Invest Ophthalmol Vis Sci*. 2005;46:2587–2591.
32. Wenzel A, Grimm C, Samardzija M, Reme CE. Molecular mechanisms of light-induced photoreceptor apoptosis and neuroprotection for retinal degeneration. *Prog Retin Eye Res*. 2005;24:275–306.

33. Grimm C, Wenzel A, Williams T, Rol P, Hafezi F, Reme C. Rhodopsin-mediated blue-light damage to the rat retina: effect of photoreversal of bleaching. *Invest Ophthalmol Vis Sci*. 2001;42:497–505.
34. Matsubara A, Nakazawa T, Noda K, et al. Photodynamic therapy induces caspase-dependent apoptosis in rat CNV model. *Invest Ophthalmol Vis Sci*. 2007;48:4741–4747.
35. Boersma HH, Kietselaer BL, Stolk LM, et al. Past, present, and future of annexin A5: from protein discovery to clinical applications. *J Nucl Med*. 2005;46:2035–2050.
36. Blankenberg FG, Strauss HW. Will imaging of apoptosis play a role in clinical care? A tale of mice and men. *Apoptosis*. 2001;6:117–123.
37. Dumont EA, Reutelingsperger CP, Smits JF, et al. Real-time imaging of apoptotic cell-membrane changes at the single-cell level in the beating murine heart. *Nat Med*. 2001;7:1352–1355.
38. Narula J, Acio ER, Narula N, et al. Annexin-V imaging for noninvasive detection of cardiac allograft rejection. *Nat Med*. 2001;7:1347–1352.
39. Zhao M, Beauregard DA, Loizou L, Davletov B, Brindle KM. Non-invasive detection of apoptosis using magnetic resonance imaging and a targeted contrast agent. *Nat Med*. 2001;7:1241–1244.
40. Laxman B, Hall DE, Bhojani MS, et al. Noninvasive real-time imaging of apoptosis. *Proc Natl Acad Sci U S A*. 2002;99:16551–16555.
41. Maass A, Lundt von Leithner P, Luong V, et al. Assessment of rant and mouse RGC apoptosis imaging in-vivo with different scanning laser ophthalmoscopes. *Curr Eye Res*. 2007;32:851–861.
42. Rosolen SG, Saint-MacAry G, Gautier V, Legargasson JF. Ocular fundus images with confocal scanning laser ophthalmoscopy in the dog, monkey and minipig. *Vet Ophthalmol*. 2001;4:41–45.
43. Zambarakji HJ, Keegan DJ, Holmes TM, et al. High resolution imaging of fluorescein patterns in RCS rat retinae and their direct correlation with histology. *Exp Eye Res*. 2006;82:164–171.
44. Hughes A. A schematic eye for the rat. *Vis Res*. 1979;19:569–588.
45. Kravtsov VD, Daniel TO, Koury MJ. Comparative analysis of different methodological approaches to the in vitro study of drug-induced apoptosis. *Am J Pathol*. 1999;155:1327–1339.
46. McMullen WW, Garcia CA. Comparison of retinal photocoagulation using pulsed frequency-doubled neodymium-YAG and argon green laser. *Retina*. 1992;12:265–269.
47. Mosier MA, Champion J, Liaw LH, Berns MW. Delayed retinal effects of the frequency-doubled YAG laser (532 nm). *Invest Ophthalmol Vis Sci*. 1987;28:1298–1305.
48. Mosier MA, Champion J, Liaw LH, Berns MW. Retinal effects of the frequency-doubled (532 nm) YAG laser: histopathological comparison with argon laser. *Lasers Surg Med*. 1985;5:377–404.
49. Roider J, Schiller M, el Hifnawi ES, Birngruber R. [Retinal photocoagulation with a pulsed, frequency-doubled Nd:YAG laser (532 nm)]. *Ophthalmologe*. 1994;91:777–782.
50. Saeed M, Parmar D, McHugh D. Frequency-doubled Nd:YAG laser for the treatment of exudative diabetic maculopathy. *Eye*. 2001;15:712–718.
51. Spaide RF, Noble K, Morgan A, Freund KB. Vitelliform macular dystrophy. *Ophthalmology*. 2006;113:1392–1400.
52. Arnold JJ, Sarks JP, Killingsworth MC, Kettle EK, Sarks SH. Adult vitelliform macular degeneration: a clinicopathological study. *Eye*. 2003;17:717–726.
53. Eckardt C, Eckardt U, Groos S, Luciano L, Reale E. Macular translocation in a patient with adult-onset foveomacular vitelliform dystrophy with light- and electron-microscopic observations on the surgically removed subfoveal tissue. *Graefes Arch Clin Exp Ophthalmol*. 2004;242:456–467.